Liquid Crystals
Publication details, including instructions for authors and subscription information:
http://www.informaworld.com/smpp/title~content=t713926090

Surface nematic liquid crystal bistability on low-symmetry photoalignment micropatterns

J. Niitsuma[a]; M. Yoneya[ab]; H. Yokoyama[ab]
[a] Liquid Crystal Nano-system Project, ERATO/SORST, Japan Science and Technology Agency, 5-9-9 Tokadai, Tsukuba, Ibaraki, Japan [b] Nanotechnology Research Institute, AIST, 1-1-1 Umezono, Tsukuba, Ibaraki, Japan

Online publication date: 12 January 2010

To cite this Article Niitsuma, J. , Yoneya, M. and Yokoyama, H.(2010) 'Surface nematic liquid crystal bistability on low-symmetry photoalignment micropatterns', Liquid Crystals, 37: 1, 31 — 36
To link to this Article: DOI: 10.1080/02678290903359283
URL: http://dx.doi.org/10.1080/02678290903359283

Liquid Crystals,
Vol. 37, No. 1, January 2010, 31–36

Taylor & Francis
Taylor & Francis Group

Surface nematic liquid crystal bistability on low-symmetry photoalignment micropatterns

J. Niitsuma[a†]*, M. Yoneya[a,b] and H. Yokoyama[a,b‡]

[a]*Liquid Crystal Nano-system Project, ERATO/SORST, Japan Science and Technology Agency, 5-9-9 Tokadai, Tsukuba, Ibaraki 300-2635, Japan;* [b]*Nanotechnology Research Institute, AIST, 1-1-1 Umezono, Tsukuba, Ibaraki 305-8568, Japan*

(Received 10 August 2009; final form 22 September 2009)

We experimentally examined the surface nematic bistability of a liquid crystal cell with four kinds of photoalignment micropatterns, including stripe, herringbone, random dots and random lamella. We checked a necessary condition on the pattern symmetry required for the bistability. The optical properties of the stripe pattern cells were compared with those of the conventional chequer pattern cells, and the effects of the pattern geometry on the optical properties were discussed. Inspired by the results of the random lamella patterns, we proposed a novel and practical method of fabricating large-area bistable patterns.

Keywords: photoalignment; micropattern; bistability; symmetry

1. Introduction

Micropatterned alignment surfaces [1–8] for liquid crystals (LCs) have been used to create characteristic LC alignment configurations that cannot be realised with a unidirectional alignment method, such as conventional rubbing. One of the most elaborate geometric patterns fabricated so far is the hexagonal combination of aligned microparallelograms, which was used for the first demonstration of a surface tristable LC device [5]. The fabrication of lower symmetric, orthogonally aligned chequer micropatterns [4, 9] has also been the subject matter of intensive study for the purpose of practical implementation of surface bistable LC devices. Because the bistable states are stored even after the switching field is turned off, these devices have received growing attention for use as LC display devices with notably reduced power consumption.

In our previous paper [10], we demonstrated that the photolithographic alignment method was of great advantage towards a high throughput microchequer patterning. The domain size (the side lengths of the constituent square domain) of the chequer pattern was as small as 1 μm. We also proposed three sufficient empirical conditions for surface bistability: (i) the pattern consists of two kinds of micron-sized domains with the local alignment directions mutually orthogonal; (ii) the anchoring energies of the two domains are balanced to realise the macroscopic alignment directions in the middle between the local orthogonal alignment directions; (iii) the pattern allows at least one symmetry (bistability-inducing symmetry, S_b) operation that exchanges the two macroscopic alignment directions to ensure their geometric equivalence. However, we should note that, being a sufficient condition, (iii) does not exclude the possibility of bistability on low-symmetry alignment patterns.

In this article, we investigate experimentally the surface bistability on such patterns with particular attention being paid to the necessity of condition (iii). The patterns examined here have a lower symmetry than the chequer pattern, only in which the bistability switching has been confirmed so far. This is motivated by the fact that if the condition is (practically) unnecessary for bistability, we will be able to obtain many more kinds of bistable patterns, including non-symmetric and non-periodic ones, facilitating the ability to find a much wider route to bistable patterning.

We apply the lithographic photoalignment method to fabricate different micropatterns, because it allows a wide variety of patterning only by using proper photomasks. Firstly, we tested bistability on one-dimensionally periodic (stripe) patterns that have S_b, and compared the optical properties with those of chequer patterns. Secondly, the stripe pattern was modified to the lower symmetric herringbone pattern without S_b and then the effect of the modification on the bistability was checked. Finally, we fabricated and tested non-periodic (random) dots and lamella patterns that possess only trivial symmetry and no S_b.

2. Experimental

Each pattern was fabricated on a polyamic acid azo film [11] by using a rewriting method [9, 10]. In this

*Corresponding author. Email: niitsuma@jaist.ac.jp

†Present address: School of Materials Science, Japan Advanced Institute of Science and Technology, 1-1 Asahidai, Nomi, Ishikawa 923-1292, Japan

‡Present address: Kent State University, Liquid Crystal Institute, P.O. Box 5190, Kent, Ohio 44242-0001, USA

ISSN 0267-8292 print/ISSN 1366-5855 online

DOI: 10.1080/02678290903359283
http://www.informaworld.com

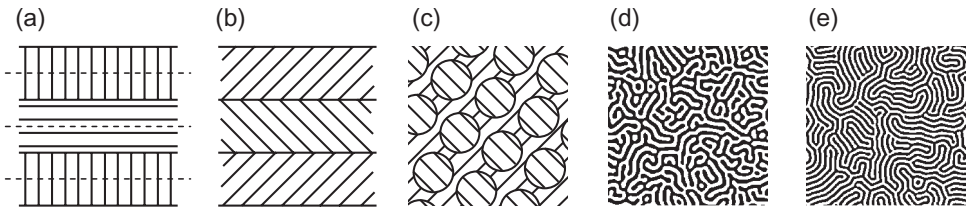

Figure 1. Schematic diagrams of the alignment patterns examined in this work: (a) orthogonal stripe (domain width = 2 and 1 μm); (b) herringbone (2 μm); (c) random dot (diameter = 0.52 μm) in which short line segments show local alignment directions; and (d), (e) random lamella patterns (widths = 2 μm) in which black and white represent two orthogonal domains. In (a), dashed lines show the mirror-reflection axes of the pattern. They have bistability-inducing symmetry because they exchange the two macroscopic alignment directions, i.e. ±45°.

process, the first (uniform) exposure of linearly polarised ultraviolet (LPUV) light (polarisation direction α) induces uniform alignment on the azo film, with the alignment direction perpendicular to α. The successive second exposure at $\alpha + 90°$ polarisation through a proper photomask rotates the azo molecule on selected irradiated areas by 90°. The appropriate second exposure dose for a fixed first exposure dose is determined so that the macroscopic stable orientation of the micropatterned alignment cell is $\alpha + 45°$ or $\alpha - 45°$ in order to satisfy condition (ii).

For the stripe patterning (Figure 1(a)) α was set at 0° with respect to the stripe direction. Grating masks with 2 and 1 μm domain sizes (line widths in this case) and 1:1 line/space ratio were used to fulfil condition (ii). For the fabrication of the herringbone pattern (Figure 1(b)) [6], which lacks S_b, α was set at –45° for the 2 μm grating masks. The resulting pattern has mirror-reflection axes on the domain boundaries. However, they are not S_b because they cannot exchange the two macroscopic alignment directions, i.e. 0° and 90°. Random dots (Figure 1(c)) were patterned through random circular apertures in chromium (Cr) film. The diameter of the aperture was 0.52 μm and the area ratio of the aperture/Cr was 1.1. To fabricate random lamella patterns (Figures 1(d) and (e)), simulations of the microphase separation of diblock copolymer [12] were carried out and the resulting two binary data were converted to two types of photomask. The area ratio of the masked/unmasked regions was set to be unity in the diblock copolymer model. The average lamella widths are ~2 μm for both patterns.

LPUV light ($\lambda = 350$–425 nm) was obtained from a Hg lamp (Ushio USH-250D) through filters and a polariser (CODIXX colorPol UV375). The irradiation energy density was 6.2 mW cm^{-2} and the first and second exposure times were 600 and 500 s, respectively. The gaps between the azo film substrates and the photomasks of ~100 nm were realised by the vacuum hard-contact method in order to avoid the diffraction effect and to enable micropatterning.

The bistable LC cell consisted of a patterned substrate at the bottom and a unidirectional alignment substrate at the top. The top substrate, prepared by exposing the whole azo film to LPUV light, had uniform alignment orientation along one of the possible bistable directions ($\alpha \pm 45°$) of the bottom substrate. The cell with a gap of 10 μm was filled with 4-*n*-pentyl-4'-cyanobiphenyl LC (5CB) in the isotropic phase. The possible nematic bistable states of the cell are homogeneous planar (H) and 90°-twisted planar (T) states. Switching between the bistable states was achieved by applying orthogonal in-plane electric fields with planar indium tin oxide (ITO) quadrupole electrodes on the bottom substrate. A rectangular ac voltage of 1 kHz frequency generated by a function generator (Agilent 33220A) followed by an amplifier (Matsusada HEOPT-3B20) was applied to an opposing electrode pair of 250 μm separation. The field-off state in the central region surrounded by the quadrupole electrodes was observed with an optical microscope (Olympus BX51) through crossed polarisers. The electric field strength was defined as the root mean square of the applied voltage divided by the electrode separation. The components ($\lambda < 480$ nm) of the illumination light were eliminated by a long-pass filter in order to avoid ultraviolet (UV) exposure during microscopy.

To compare the optical properties between the orthogonal stripe patterns and the chequer patterns, the contrast ratio (CR) was evaluated. Because the switching area was too small to measure the light intensity of the H and T states, we used the dark and bright intensity of a large-area H state region of the cell between the crossed and parallel polarisers, which was measured by a photodetector (New Focus 2031) with a digital multimeter (Agilent 34401A).

3. Results and discussion

3.1 Orthogonal stripe pattern

Figure 2 shows optical micrographs of the 2 μm horizontal stripe pattern LC cell in switching. The dark

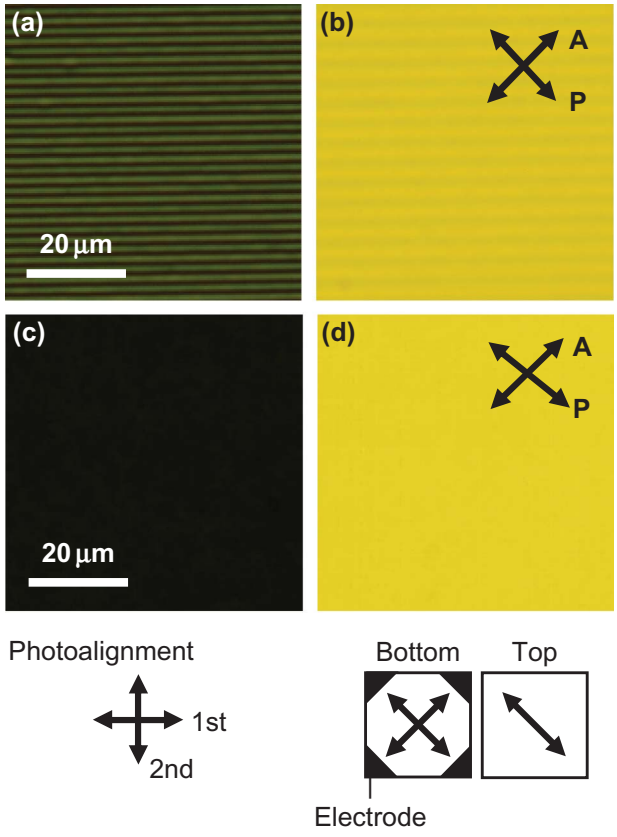

Figure 2. Polarising optical micrographs of the bistable states of a 2 μm horizontal stripe pattern cell in (a) the H state and the (b) T state. (c), (d) Corresponding images of the 1 μm stripe pattern cell. The arrows labelled P and A indicate the polariser and analyser directions, respectively. Also shown are the first and second photoalignment directions, and the alignment axes on the bottom and top substrates of the bistable cell. The filled triangles at the corners of the bottom substrate indicate the arrangement of quadrupole electrodes for switching.

and bright states correspond to the H and T states, respectively. The average switching field strength E_{sw} was ~2 V_{rms} μm^{-1} and the estimated CR was 5.3:1. The results demonstrated the switching between the bistable states, which had been expected because this type of geometry has a mirror-reflection axis as S_b is in the middle of each stripe domain (Figure 1(a)). Similar results were obtained for the 1 μm stripe pattern cell (Figures 2(c) and (d)) with E_{sw} of ~3 V_{rms} μm^{-1} and a CR of 16:1. The stripe textures of the 1 μm cells in the H and T states could not be resolved by optical microscopy.

The average switching field strengths of the stripe cells ~3 V_{rms} μm^{-1} were smaller in comparison with that of the chequer pattern (~6 V_{rms} μm^{-1}) of the same domain sizes fabricated under the same experimental conditions (not shown). To explain the result, we noted the difference in the switching process between the two patterns. For the latter cells, the switching in the central region surrounded by the electrodes occurs in a uniform in-plane electric field. On the other hand, for the former cells, every stripe domain is extended to the electrodes at which the inhomogeneous electric field (which is much stronger than that of the observation region) is generated. As a result, the switching of the microstripe pattern was first set off near an electrode edge at a low applied voltage, and then the switching boundary moved along the stripe domains at a speed of ~200 μm s^{-1}. We could observe the movement even after the electric field was turned off. This accounts for the apparent small E_{sw} for the stripe pattern cells. In any case, the results of the microstripes suggest the possibility of further reducing the E_{sw} of a cell due to a characteristic arrangement of the pattern and switching electrodes.

We next consider the reasons for the difference in the measured CR. We think that there are two mechanisms that determine the CR. The first is the behaviour of the LC director near the alignment surface. The local LC alignment on the patterned surface relaxes exponentially to a macroscopically uniform state with a different length scale a, depending on the domain size d. For the stripe pattern cell of an infinite thickness with 5CB, $a_{stripe} = \kappa d/\pi \sim 0.2d$, where $\kappa^2 = K_{22}/K_{11} \sim 0.5$ [13]. (We assume here that $K_{11} = K_{33}$ for simplicity. K_{11}, K_{22} and K_{33} are the splay, twist and bend elastic constants of the LC.) When a_{stripe} is smaller than the visible light wavelength, the local LC texture cannot be resolved by optical microscopy, resulting in a high CR. This is the case of the 1 μm stripe, as shown in Figures 2(c) and (d), because a_{stripe} ~ 200 nm, while the relaxation effect is not so large for the 2 μm pattern because a_{stripe} ~ 400 nm. The second mechanism is the contribution from the domain boundary regions. The LC alignment orientation on the domain boundary is always directed along the average direction between the two adjacent orthogonal alignment domains, i.e. one of the macroscopic bistable directions. This appears as the brightest (darkest) lines in the T (H) state of Figure 2(a) (Figure 2(b)) with clarity and contributes to the contrast. It is obvious that the high areal density of the boundary for small domain size enhances the contrast.

We compare the CR between the stripe and the chequer pattern cells in Table 1. It is found that, for the same domain size, the chequer pattern cell showed better performance than the counterpart of the stripe pattern cell. This result also supports the above two contrast mechanisms because, for the same d, $a_{chequer} = a_{stripe}/\sqrt{2} < a_{stripe}$ [10] and the areal density of the boundary, ρ, of the chequer is higher than that of the stripe. We define a figure of merit as ρ/a in order to evaluate the dependence of the CR on pattern geometry. Figure 3 shows the result and the figure of merit is

Table 1. Measured CR k:1 of the stripe and checker pattern cells with domain sizes of 2 and 1 μm.

	Domain size	
k	2 μm	1μm
Stripe	5.3	16
Checker	8.2	30

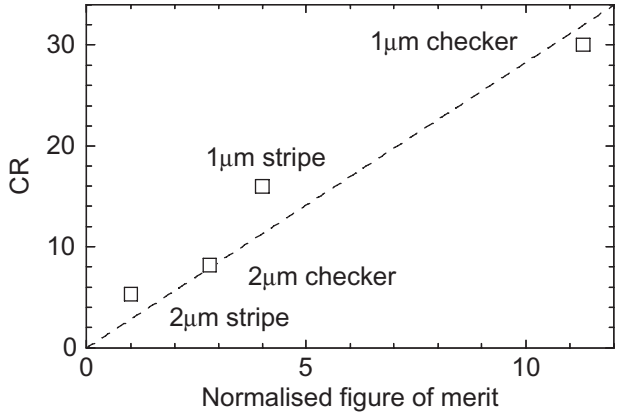

Figure 3. The dependence of the CR on a figure of merit normalised to the value of a 2 μm stripe pattern cell. The dashed line is a guide for the eye.

found to be a good measure of the CR for the present experimental results.

3.2 *Herringbone pattern*

Figure 4 shows the results of the switching of the herringbone pattern cell ($E_{sw} \sim 1$ V_{rms} μm^{-1}) and clearly manifests that the bistability occurred even in this pattern. Therefore, it is proved that the presence of S_b is not necessary for the bistability. A detailed examination reveals that the energetic degeneracy of the two bistable states in a thick cell is automatically guaranteed only by conditions (i) and (ii) in the following way. Bearing in mind that the nematic LC director $\boldsymbol{n}$ has the property $\boldsymbol{n} = -\boldsymbol{n}$, we obtain four-fold degenerate states, $(\boldsymbol{n}_1, \boldsymbol{n}_2)$, $(-\boldsymbol{n}_1, \boldsymbol{n}_2)$, $(\boldsymbol{n}_1, -\boldsymbol{n}_2)$ and $(-\boldsymbol{n}_1, -\boldsymbol{n}_2)$, where $\boldsymbol{n}_1$ and $\boldsymbol{n}_2$ are the surface directors of the orthogonally aligned two microdomains (condition (i)). Because the macroscopic $\pi/2$ switching (condition (ii)) is caused by the buckling [4], i.e. the π rotation of either of the surface director $\boldsymbol{n}_1$ or $\boldsymbol{n}_2$, the four-fold degeneracy becomes macroscopically two fold or bistable: $(\boldsymbol{n}_1, \boldsymbol{n}_2) = (-\boldsymbol{n}_1, -\boldsymbol{n}_2)$ and $(-\boldsymbol{n}_1, \boldsymbol{n}_2) = (\boldsymbol{n}_1, -\boldsymbol{n}_2)$.

3.3 *Random dot pattern*

The switching behaviour of the random dot pattern cell is shown in Figure 5. Based on the above results,

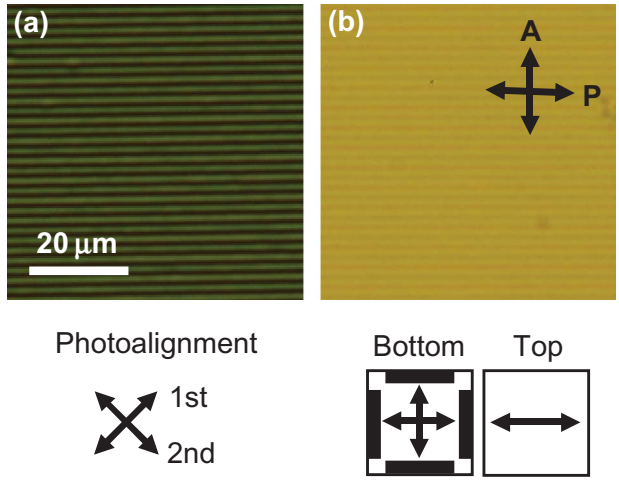

Figure 4. Polarising optical micrographs of bistable states of a 2 μm herringbone pattern cell: (a) H state and (b) T state.

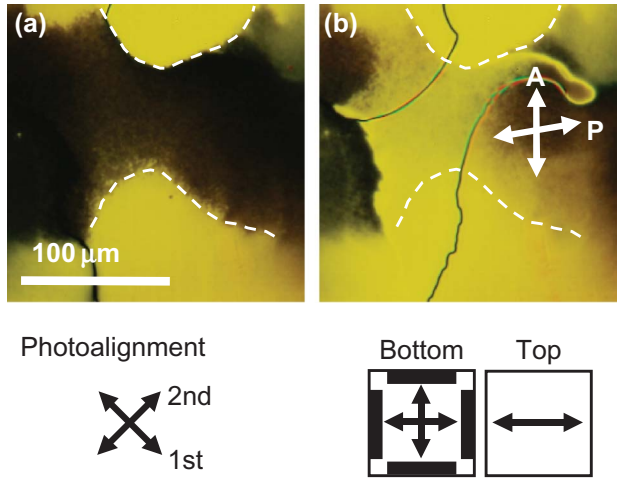

Figure 5. Large-area polarising optical micrographs of the bistable states of a random dot pattern cell: (a) the H state and (b) the T state. The switching areas are bounded by white dashed curves in the centre of the images, where darkness or brightness is not perfect compared with the surrounding regions.

the pattern is also expected to be bistable and we can see a change in brightness at ~5 V_{rms} μm^{-1}. However, the results in Figure 5 show the imperfect darkness and brightness in the central regions compared with the optical properties in the surrounding area (even at ~10 V_{rms} μm^{-1}, the maximum electric field we could use). An observation revealed that the surface alignment orientation in the central region was not in bistable directions, i.e. ±45°, but ~15° with respect to the alignment direction induced by the first LPUV light exposure. This fact indicates that the pattern was not completely rewritten and did not fully satisfy condition (ii), which leads us to examine the diffraction intensity of the LPUV light in the photolithography process.

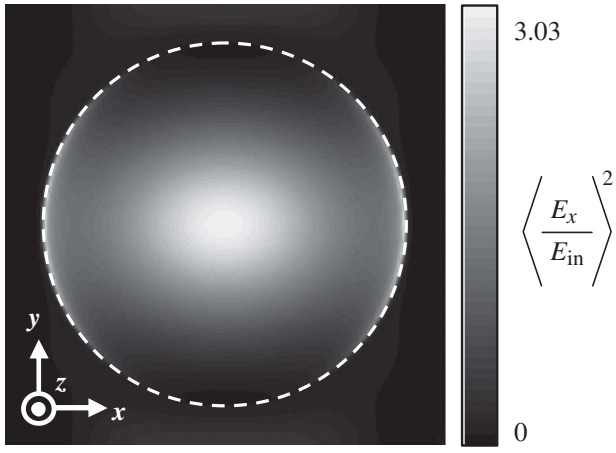

Figure 6. Simulated time-average spatial intensity profiles of electric fields transmitted through a circular aperture in Cr film at gap distances of 100 nm. Incident light (λ= 365 nm) with unit intensity is polarised along the x-axis and travels along the z-axis. The white dashed circle indicates the aperture rim.

Figure 6 shows a simulated time-average spatial intensity profile of LPUV light passing through a Cr circular aperture mask at the actual gap distance of 100 nm. The simulations were carried out by a finite-difference time-domain method (Rsoft FullWAVE) under the periodic boundary conditions. The intensity was normalised to that of a monochromatic incident light (λ= 365 nm). As shown in this figure, the intensity of the diffraction field is weak around the upper and bottom rims, i.e. the rims parallel to the incident electric field. Such near-field patterns are common features in the diffraction through circular apertures [14]. Because the photoalignment film around the two rim regions will not be exposed, we could say that this is the reason for the incomplete rewriting. The current example demonstrates that a circular aperture is not suitable for the fabrication of dot patterns by the rewriting method with LPUV light.

3.4 *Random lamella pattern*

Figure 7 shows the results of the bistable switching of random lamella patterns. There were no essential differences in the switching behaviour and the switching field $\sim$2 V_{rms} μm^{-1} between the two lamella patterns (Figures 1(d) and (e)). Any imperfect darkness or brightness, as shown in Figure 5, was not observed here, except for the inhomogeneous optical features observed along each winding domain reflecting the variation in the domain width w. These are clear examples of the bistability on random patterns. The distinct dark–bright switching could be ascribed to the fact that the intensities of the LPUV light passing through

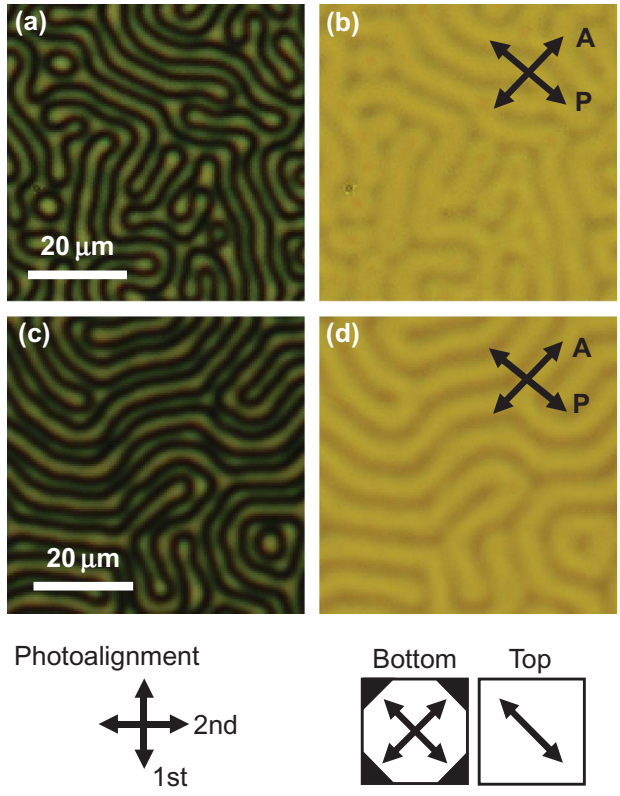

Figure 7. Polarising optical micrographs of bistable states of the cell of the random lamella pattern of Figure 1(d) in (a) the H state and (b) the T state. (c), (d) Corresponding images of the lamella of Figure 1(e).

the lamella patterned masks are homogeneous over the domains, which was confirmed by a simulation.

The experimental verification of the bistability on the random lamella patterns let us propose a novel way of fabricating large-area patterns for bistability by using a microphase separation film of a real diblock copolymer material. Photoalignment polymers are divided into two types, depending on whether they show perpendicular or parallel alignment with respect to the polarisation direction of exposed LPUV light [15]. When a diblock copolymer is synthesised from these two types of polymers as two subunits, and if it forms microphase separation patterns (as in Figures 1(d) or (e)), we could easily obtain a bistable pattern simply by exposing it to uniform LPUV light. This is a one-shot process and no photomask is needed. A careful design and preparation of the microphase separation film will be essential to satisfy condition (ii). For example, the segregated two phases of the polymers should result in the equivalent anchoring energy density for the same LPUV light dose, which might requires the development of new photoalignment polymers suitable for this purpose.

4. Summary

We have examined surface bistability for the LC cell with four kinds of micropatterned alignment, including stripe, herringbone, random dots and random lamella, by using the photoalignment method to check the necessary condition on the pattern symmetry required for the bistability.

As a result, the stripe patterns (having S_b) showed bistability and the herringbone pattern (not having S_b) also became bistable. The result drew an important conclusion that the geometric symmetry condition is not necessary for bistability on microstructured alignment. This was also confirmed with the random dot and lamella patterns. For the random dot pattern, however, the observed bistability was not perfect because the rewritten areas were smaller than we had expected, because of a characteristic LPUV diffraction pattern through circular apertures in the photomask.

We also evaluated the pattern dependency of the CR of the cell. The CR of the stripe pattern was lower than that of the chequer pattern for the same domain size. This was explained by the following two facts: (1) the local LC alignment on the patterned surface relaxes exponentially to a macroscopically uniform state with a different length scale that is proportional to the domain size; (2) the high density of the boundary for small domain size enhances the contrast.

Lastly, inspired by the bistability on the random lamella pattern, we propose a novel method of fabricating large-area patterns for bistability by using the microphase separation of a diblock copolymer with a specified material design. The implementation of this one-shot maskless photoalignment patterning may be a great challenge in the future.

Acknowledgements

The authors thank Mr. M. Uchishima of Nikon and Mr. T. Mushu of Pulstec Industrial for their work on photomask fabrication. J.N. thanks Dr. Y. Mitsuhashi for his continuous encouragement.

References

[1] Gupta, V.K.; Abbot, N.L. *Science* **1997**, *276*, 1533–1536.
[2] Lee, B.-W.; Clark, N.A. *Science* **2001**, *291*, 2576–2580.
[3] Crawford, G.P.; Eakin, J.N.; Callan-Jones, A.; Pelcovits, R.A. *J. Appl. Phys.* **2005**, *98*, 123102-1–123102-10.
[4] Kim, J.-H.; Yoneya, M.; Yamamoto, J.; Yokoyama, H. *Appl. Phys. Lett.* **2001**, *78*, 3055–3057.
[5] Kim, J.-H.; Yoneya, M.; Yokoyama, H. *Nature* **2002**, *420*, 159–162.
[6] Batalioto, F.; Bechtold, I.H.; Oliveira, E.A.; Evangelista, L.R. *Phys. Rev. E* **2005**, *72*, 031710-1–031710-4.
[7] Gwag, J.S.; Fukuda, J.; Yoneya, M.; Yokoyama, H. *Appl. Phys. Lett.* **2007**, *91*, 073504-1–073504-3.
[8] Bramble, J.P.; Evans, S.D.; Henderson, J.R.; Anquetil, C.; Cleaver, D.J.; Smith, N.J. *Liq. Cryst.* **2007**, *34*, 1059–1069.
[9] Niitsuma, J.; Yoneya, M.; Yokoyama, H. *Appl. Phys. Lett.* **2008**, *92*, 241120-1–241120-3.
[10] Niitsuma, J.; Yoneya, M.; Yokoyama, H. *Jpn. J. Appl. Phys.* **2009**, *48*, 040201-1–040201-3.
[11] Park, B.; Jung, Y.; Choi, H.-H.; Hwang, H.-K.; Kim, Y.; Lee, S.; Jang, S.-H.; Kakimoto, M.; Takezoe, H. *Jpn. J. Appl. Phys.* **1998**, *37*, 5663–5668.
[12] Bahiana, M.; Oono, Y. *Phys. Rev. A* **1990**, *41*, 6763–6771.
[13] Hakemi, H.; Jagodzinski, E.F.; DuPré, D.B. *J. Chem. Phys.* **1983**, *78*, 1513–1518.
[14] Martin, O.J.F.; Paulus, M. *J. Microsc.* **2002**, *205*, 147–152.
[15] O'Neill, M.; Kelly, S.M. *J. Phys. D. Appl. PhyS.* **2000**, *33*, R67–R84.